J. Fluid Mech. (1983), *vol.* 127, *pp.* 315–339
Printed in Great Britain

On the mechanism of Korotkoff sound generation at diastole

By M. SHIMIZU AND Y. TANIDA
Institute of Interdisciplinary Research, University of Tokyo

(Received 5 November 1981 and in revised form 18 June 1982)

In the auscultatory technique, the most widely used clinical method to measure the arterial blood pressure, the systolic and diastolic blood pressures are estimated based on the beginning and cessation of the so-called Korotkoff sound emitted from the artery. Despite the widespread use of the technique, the mechanism by which Korotkoff sound is generated has not been well understood. In this report, a series of model experiments and a one-dimensional wave-propagation analysis have been conducted in order to elucidate the mechanism. As a result, the clear thud sound, heard when the cuff pressure is in the vicinity of the diastolic blood pressure, has been found to be generated by the sudden expansion of the vessel due to the shock wave that is formed at the wave front by compression-wave overtaking during wave propagation through the partially collapsed vessel segment under the cuff. Because of the strong nonlinear characteristics of the tube law, the sudden change in the vessel compliance around the near-zero transmural pressure, the shock wave is formed only when the cuff pressure, externally applied to the vessel, is nearly equal to or higher than the diastolic blood pressure and the vessel is partially collapsed in the late diastolic phase. The shock strength at the distal end of the partially collapsed vessel segment increases with the cuff pressure and the collapsed-vessel segment length within some limits. The waveform of the sound is well correlated with the time differential of the pressure waveform.

1. Introduction

The arterial blood pressure is one of the most significant diagnostic parameters in clinical medicine. The most widely used non-invasive clinical method for blood-pressure measurement is the so-called auscultatory technique, which uses a pneumatic cuff and a manometer monitoring the cuff pneumatic pressure. In this method, systolic and diastolic blood pressure are estimated as follows. The cuff set on an upper arm is at first inflated rapidly above the systolic pressure to stop the arterial blood flow completely and is then deflated gradually. As the cuff pressure drops to a certain critical limit, clear short tapping sounds become audible with each pulse through a stethoscope set right above the brachial artery distal to the cuff. With further decrease of the cuff pressure, the tapping sounds change into murmurs and then into clear thud sounds and finally all sounds disappear. The cuff pressures at which the first tapping sound and the last thud sound are heard are commonly selected as the systolic and the diastolic arterial blood pressure respectively. The sounds mentioned above are called Korotkoff sounds because the auscultatory technique was first proposed by Korotkoff (1905).

This method has been empirically proved to be valid in the majority of persons under normal conditions (errors arise with obese patients, the use of a cuff of

inappropriate size, etc.) by a great number of clinical studies conducted since its introduction in the early 20th century in which non-invasively determined systolic and diastolic pressures were compared with directly measured ones (Pickering 1955).

However, the mechanism by which Korotkoff sound is generated has not yet been understood. Since understanding of the reason why clear tapping or thud sounds are emitted from such a pliable tube as a blood vessel is not only interesting from the scientific point of view, but also indispensable for improving the method's reliability and expanding its availability, many attempts to elucidate the mechanism have been conducted. Erlanger (1921) observed an increase in the steepness of the ascending limb of the pulse and small high-frequency waves appearing in front of it, when the pulse propagates through a canine carotid artery compressed pneumatically and partially collapsed. He termed it the preanacrotic phenomenon. Stimulated by Erlanger's study, Bramwell (1925) constructed a model artery with the inner tube of a bicycle tyre and studied deformation of the pulse wave when it propagates through the collapsed tube and obtained similar results to those of Erlanger. Bramwell tried to explain the preanachrotic phenomenon as closely analogous to the formation of a shock wave and breakers in the case of waves on the seashore. In the end, however, he concluded that Korotkoff sound was generated by the turbulence produced by instability of the wave front. His idea of shock-wave formation was supported only by Beam (1968), who showed analytically the development of the shock wave and proposed the latter as the cause of the short sharp sound. The shock-wave hypothesis, however, has been neglected by all other researchers, and several other hypotheses to explain rapid vessel-wall vibration were proposed, such as the excitation due to turbulent flow (Chungchareon 1964; Burns 1959; Fruehan 1962), instability of a partially collapsed tube filled with incompressible fluid (Anliker & Raman 1965) and nonlinear limit-cycle oscillation observed when fluid flows through a tube, a portion of which is compressed by excess external pressure (Ur & Gordon 1970; Lighthill 1972). But all of them except Beam's failed to explain the deformation of the pulse wave; when Korotkoff sound is heard, the pulse wave monitored in the artery distal to the cuff is deformed greatly and always has a very steep ascending limb with which Korotkoff sound synchronizes (Wallace, Lewis & Khalil 1961).

From the experimental studies conducted by various researchers, the following facts are known: (i) Korotkoff sound is heard only when the cuff pressure is between systolic and diastolic pressure, and hence the blood vessel below the cuff is partially collapsed in late diastolic phase (MuCutcheon & Rushmer 1967); (ii) the tapping and thud sound is produced in a short period synchronizing with the ascending limb of each pulse coming out from the collapsed-vessel segment, which is extraordinarily steeper than that of a normal pulse (Wallace *et al.* 1961). Furthermore, analytical studies of pressure-wave propagation through such an elastic tube as a blood vessel or thin-walled rubber tube filled with incompressible fluid show that the propagation velocity of a small perturbation is decreased as the transmural pressure of the vessel decreases, therefore a finite-amplitude compression wave (ascending limb of the pulse wave) becomes steeper as it propagates (Bramwell 1925; Kamm & Shapiro 1979). Since the compliance of such tubes increases abruptly as they begin to collapse under the condition of negative transmural pressure (Brower & Scholten 1975), the ascending limb of the pulse wave travelling through the partially collapsed vessel segment is considered to steepen rapidly and to produce a pressure discontinuity surface (shock wave) in a short propagation distance.

These facts and considerations led us to consider the shock wave as a most likely

source of the tapping or thud sound. In order to prove this hypothesis, model experiments and an analytical study were conducted and, as a result, Korotkoff sound at diastole (that is, when the cuff pressure is around the diastolic blood pressure level) has been shown to be generated by the shock formed in the partially collapsed tube. The details will be discussed in the following sections.

2. Experimental apparatus and procedure

In the planning of the experimental apparatus, the following consideration was made so that the real situation was simplified.

The form of the real pulse wave at some location of the brachial artery is determined as a result of interaction of incident wave and reflection waves from various distal locations of the arterial system. However, as mentioned in §1 Korotkoff sound is generated in a short period synchronizing with the ascending limb of each pulse, in which the incident wave is dominant. This suggests that the incident wave plays the main role in sound generation. Therefore in the experiment reflection from locations distal to the cuff is neglected.

When the cuff is inflated, reflection waves may be produced at the cuff. They propagate up the artery and are re-reflected at many locations, such as the junction of the aorta and the heart, and come back to the cuff location, changing the incident pressure waveform. The effect of these waves can be important, but the real arterial system is too complicated to allow estimation of the magnitude and the shape of the waves. Therefore these waves are also neglected in the experiment and the incident pressure waveform is assumed to be the same in both cases with and without cuff compression.

The situation of late diastolic phase is considered to be quasi-steady as the blood-flow velocity is very low compared with that due to the main part of the pulse wave. Therefore in the experiment the blood flow at late diastole is neglected and the situation is assumed to be stationary.

In the real situation, the vessel external pressure applied by the cuff has a gradual distribution along the vessel axis, caused by the rounded ends of the cuff and the tissue between the cuff and the vessel. But it is not easy to determine the real external-pressure distribution, which may change from subject to subject. Therefore, in order to avoid complication, the most primitive case – sudden change of vessel external pressure at the cuff margins – was selected.

The experimental apparatus is shown in figure 1 (*a*). It consists of a thin-walled latex penrose rubber tube of 9 mm diameter, a pressure box and a mechanical pump, which simulate an artery, a pneumatic cuff and the heart respectively. Water is selected as the working fluid. The total length of the rubber tube is 2·3 m. The rubber tube penetrates the pressure box, which is set on the central portion of the tube, through 9 mm holes drilled on each of the box sidewalls (5 mm thick) and glued to them. The proximal and distal ends of the tube are connected to the pump and the water reservoir 1 respectively. The initial internal pressure P_0 of the tube, corresponding to the diastolic pressure, is set arbitrarily by changing the height of the reservoir. Several pressure taps for measuring the static pressure P in the tube are set on the bottom of the tube as shown in figure 1 (*b*). Therefore the tube segment in the box is fixed on its bottom to the base plate at 4 or 6 pressure-tap locations and hence partially restricted in its axial movement. The other part of the tube segment, however, is completely free. Locations of the pressure taps are represented by X, which is the distance along the tube axis from the inner surface of the proximal

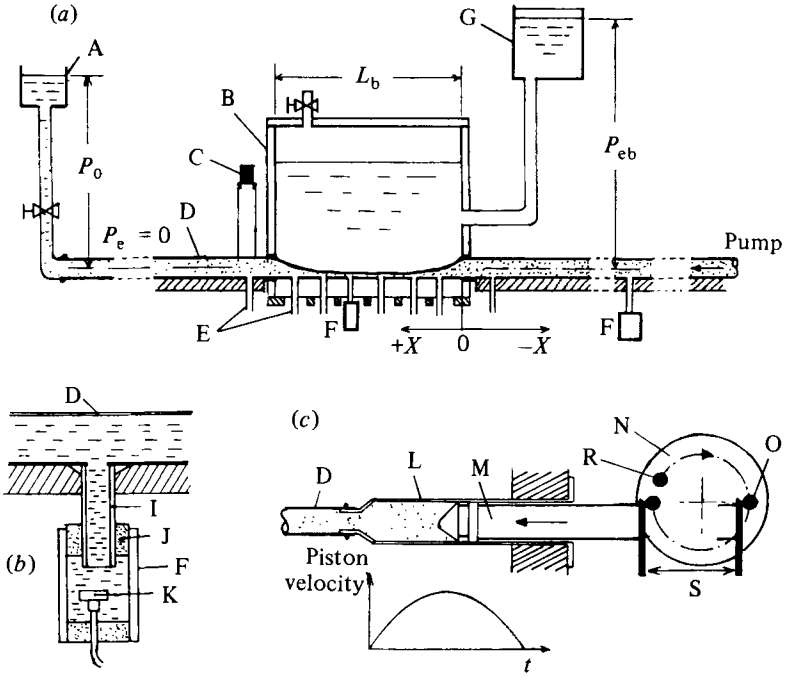

FIGURE 1. Experimental apparatus: (*a*) schematic diagram of apparatus; (*b*) detail of pressure tap and pressure-transducer system; (*c*) detail of mechanical pump. A, water reservoir 1; B, pressure box; C, microphone; D, rubber tube; E, pressure taps; F, pressure-transducer box; G, water reservoir 2; I, brass tube; J, hard rubber cork; K, pressure transducer; L, injector; M, piston; N, rotating disk; O, pin pusher; R, pin initial position.

pressure box wall. X is negative in the proximal direction and positive in the distal direction.

Two small sensitive strain-guage-type pressure transducers are used to measure P. One is always set on the reference site, 44 cm proximal to the pressure box, and the other on any other tap.

The pressure box is connected to the water reservoir 2 and the pressure P_{eb} in the box, representing the cuff pressure, is arbitrarily set by changing the height of the reservoir. The pressure box always contains a certain amount of air and water to simulate the pneumatic cuff and the tissue of the upper arm respectively. The length L_b of the box used in this study is 19 or 9 cm.

Details of the pump are shown in figure 1 (*c*). The pump consists of a commercially available plastic injector and a pin pusher, which is set vertically on a disk rotating at constant speed, and pushes the injector piston only once. Therefore, as shown in the figure, the piston velocity variation with time and hence the pressure wave generated in the rubber tube are half-sinusoidal. The amplitude and period of the pressure wave can be set arbitrarily by changing the piston stroke S and the rotation speed N of the pin pusher. The flow rate Q produced by the pump is expressed as $Q(t) = 5{\cdot}85NS \sin 2\pi Nt$.

The sound generated by the pressure wave is monitored by a condenser-type microphone at some locations distal to the pressure box. The microphone is set on one end of a plastic tube, of which the other end is made semicircular and is in contact with the rubber tube.

Movement of the top of the rubber tube wall due to the pressure wave is measured

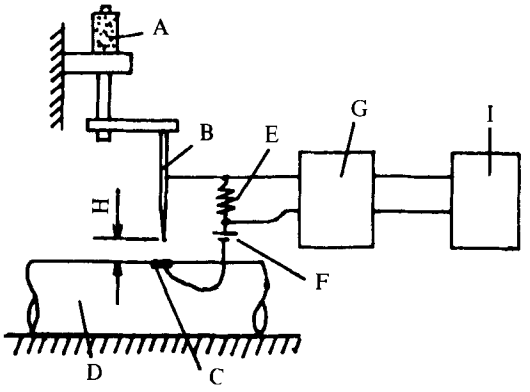

FIGURE 2. Schematic diagram of wall-displacement measuring system. A, micrometer; B, needle; C, metal foil; D, rubber tube; E, electrical resistance; F, battery; G, data recorder; I, pen recorder.

at the same location where sound is monitored. The apparatus measuring the wall movement is shown in figure 2. A small thin metal foil is glued on the top of the rubber tube and a metal needle is set vertically right above the foil. The foil, the needle, a battery and a resistance make an electric circuit. In this system, the electric current is detected only when the tube is inflated by the pressure wave and the foil and the needle tip touch each other, therefore the contact period can be detected. By changing the initial clearance H between the needle tip and the foil and repeating the same experiment, the tube-wall movement is determined.

All the pressures are measured based on the atmospheric pressure. The whole rubber tube except the segment in the pressure box is in the atmosphere, therefore the external pressure P_e outside the pressure box is zero everywhere. In order to raise frequency responsiveness of the recording system, all data are stored on a seven-channel data recorder and played back at a speed of $\frac{1}{16}$ of the recording speed for data processing.

3. Experimental results

3.1. *Tube law*

The tube law, which is expressed by the relation between tube cross-sectional area A and transmural pressure $P-P_e$, plays an essential role in pressure-wave propagation through an elastic tube filled with fluid. From this reason, the tube law of the rubber-tube segment in the pressure box was measured first of all as shown in figure 3. Here A is the mean value within the pressure box determined by dividing the segment volume by its length L_b. The filled and open circles in the figure correspond to the pressure box of 19 and 9 cm length respectively. In both cases, when $P-P_{eb}$ is large, and hence the rubber tube is fully inflated, the tube compliance $K = dA/d(P-P_{eb})$ is small, but, when $P-P_{eb}$ becomes nearly zero or slightly negative, K increases abruptly along the tube collapse. When $P-P_{eb}$ decreases further and the upper and lower tube walls contact at the centre, K again decreases gradually. The dependence of the tube compliance on the box length L_b over the negative $P-P_{eb}$ range is considered to be due to the end effect; near the ends of the collapsed tube segment, it is fixed to the holes in the solid walls, maintaining a circular shape, which restricts tube collapse.

In the figure, the wave-propagation velocity ($C = (A/\rho K)^{\frac{1}{2}}$) of a small perturbation,

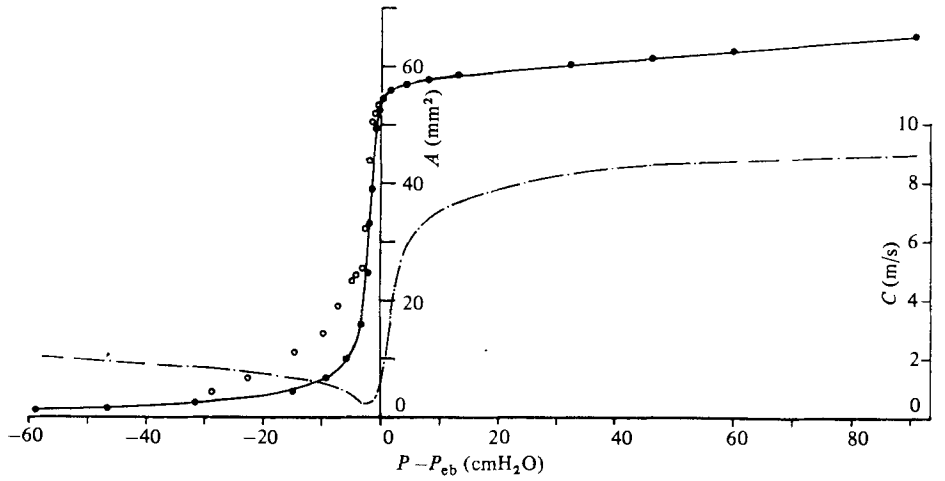

FIGURE 3. Tube law and perturbation-propagation velocity of the tube segment in the pressure box: ●, tube law for $L_b = 19$ cm; ○, tube law for $L_b = 9$ cm; —·—, C for $L_b = 19$ cm.

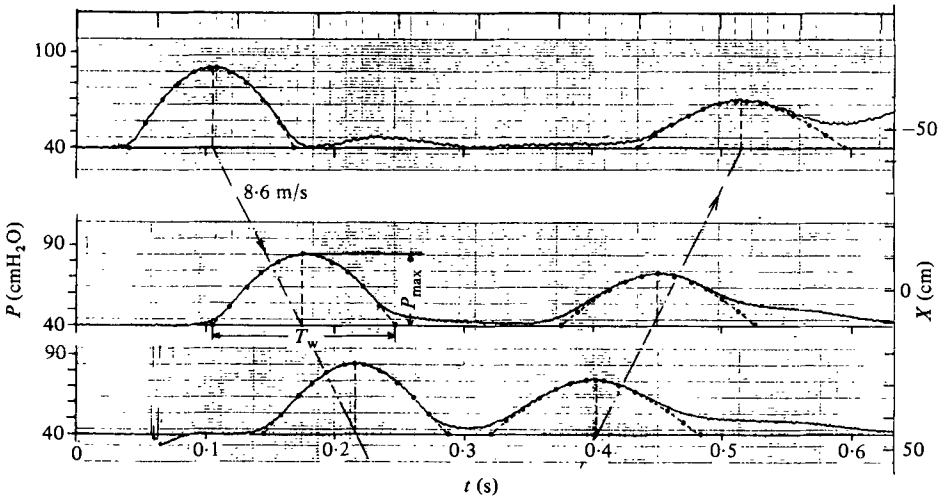

FIGURE 4. Measured pressure wave at three locations for $P_{eb} = 0$ and best-fitted half-sinusoidal curves; $L_b = 19$ cm, $P_0 = 40$ cmH$_2$O: —●—, best-fitted half-sinusoidal curve; top, $X = -44$; middle $X = 11$; bottom, $X = 46$ cm.

determined from the filled-circle data, is shown as a reference. As observed by many researchers, C decreases significantly along with tube collapse and the minimum value is only 0·46 m/s.

3.2. *Deformation of pressure wave*

3.2.1. *Case without the external pressure in the box,* $P_{eb} = 0$. At first the basic characteristics of pressure-wave propagation when none of the tube is compressed externally was examined. Time variation of the tube internal pressure P due to the propagating pressure wave was measured at various locations along the tube axis. An example of the pressure waveforms measured at three locations is shown in figure 4, where the initial tube pressure $P_0 = 40$ cmH$_2$O, flow rate of the pump $Q(t) = 45 \sin 24{\cdot}4t$ cm^3/s, and pressure-box length $L_b = 19$ cm. The figure indicates

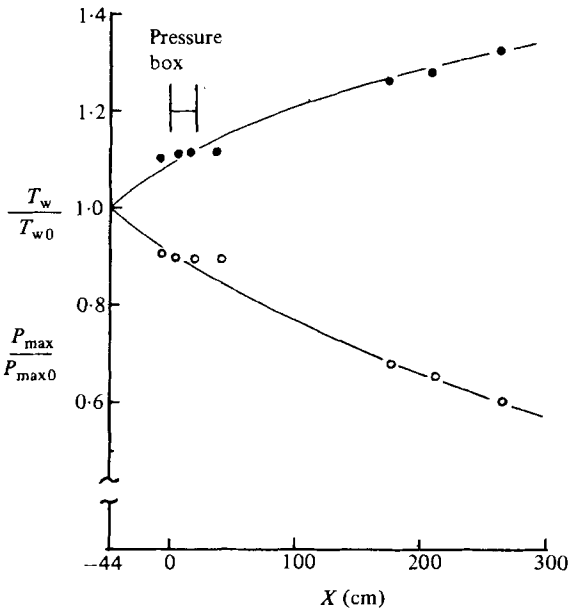

FIGURE 5. Change of P_{max} and T_w for $P_{eb} = 0$: ●, T_w/T_{w0}; ○, P_{max}/P_{max0}.

that the half-sinusoidal pressure wave generated by the pump propagates in the distal direction (the left hump in each of the three records) and is reflected at the distal end of the tube closed by the valve and then propagates in the opposite direction (the second humps). In the course of propagation, the maximum pressure amplitude P_{max} decays and the foot of the wave expands widely, whereas the main part of the pressure wave maintains the half-sinusoidal form and the steepening phenomenon is not observed. The wave propagation velocity W, determined from the P_{max} movement, does not depend on X and is about 8·6 m/s, which agrees well with the calculated perturbation-propagation velocity C shown in figure 3.

In order to know the characteristics of pressure-wave deformation, the main part of each pressure wave was approximated by the best-fitted half-sinusoidal curve as shown in figure 4 by dotted broken lines. P_{max} and the pressure wave width T_w, which is represented by a half-period of the sinusoidal curve, are plotted against X in figure 5, where P_{max0} and T_{w0} are the values at the reference site $X = -44$ cm. The data on P_{max} and T_w over X greater than 150 cm are obtained from the reflected pressure wave. Surveying over a wide range of X, P_{max} decays and T_w widens with increasing X, probably owing to viscous effects, but in the vicinity of the pressure box, which becomes the main test section in the following experiments, they are kept almost constant, and hence the pressure waveform changes little. From these experimental results it can be said that, when the tube is fully inflated, the pressure waves as strong as those treated in this experiment can be regarded as small perturbations, which can be treated by linearized theory.

The pressure waves measured at the reference site ($X = -44$ cm) and in the vicinity of the 19 cm pressure box ($X = -1·5$, 20·5, 35·5 cm) and the sound monitored at 1·5 cm distal to the pressure box ($X = 20·5$ cm) are shown in figure 6. The experimental conditions are the same as those in figure 4. As seen in the figure, the sound synchronized with the pressure wave can be detected by the microphone, but not heard by the ear set at the end of the plastic tube instead of the microphone. It is

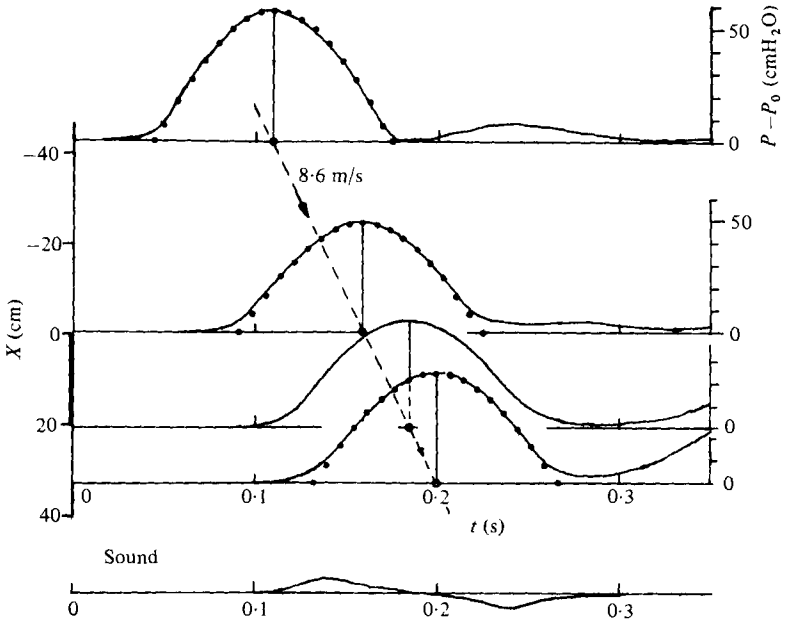

FIGURE 6. Measured pressure wave in the vicinity of the pressure box and sound monitored at the exit of the box; $L_b = 19$ cm, $P_0 = 40$, $P_{eb} = 0$, $P_0 - P_{eb} = 40$ cmH$_2$O. The top four figures are pressure and the bottom one is sound. Measuring site, from top to bottom, $X = -44$, $-1{\cdot}5$, $20{\cdot}5$, $35{\cdot}5$, $20{\cdot}5$ cm.

considered to be due to the very low amplitude of audible sound components higher than 20 Hz.

3.2.2. *Case with P_{eb} a little higher than the initial tube internal pressure P_0.* In order to know the effect of tube collapse in the pressure box on pressure-wave propagation, a series of experiments have been conducted by setting the initial transmural pressure $P_0 - P_{eb}$ in the pressure box to be in the sudden A-change region in figure 3, which simulates the condition of diastolic-pressure measurement in the auscultatory technique.

The pressure wave and sound measured at the same locations as in figure 6 are shown in figure 7 for $P_0 - P_{eb} = -0{\cdot}8$ cmH$_2$O. All the experimental conditions other than P_{eb} are the same as those in figure 6 (the pressure waves from figure 6 are shown in figure 7 by broken lines for comparison). Pressure waves at every measurement site are greatly deformed from those of the fully inflated tube case. Since, among all the experimental conditions the only change is in P_{eb}, which compresses and squeezes the tube segment in the pressure box, the pressure-wave deformation should be caused by the partially collapsed tube segment. Therefore the deformation observed on the proximal side to the pressure box is logically inferred to be caused by the reflection wave from the collapsed segment in the box. Since it is known that the pressure-wave propagation in the fully inflated tube can be treated linearly, the reflection wave can be calculated by subtracting the incident wave (pressure wave indicated by broken lines) from the resultant wave (indicated by solid lines). The reflection waves at $X = -1{\cdot}5$, -44 cm, obtained graphically, are shown in figure 8. The dotted line in the upper figure is the reflection wave at $X = -1{\cdot}5$ cm shown for comparison. The close resemblance between the two should be noted. The wave-propagation velocity determined from the shift of the peak is 8·2 m/s, which is a little smaller than that of the incident pressure wave (8·6 m/s). The difference is considered to be caused by

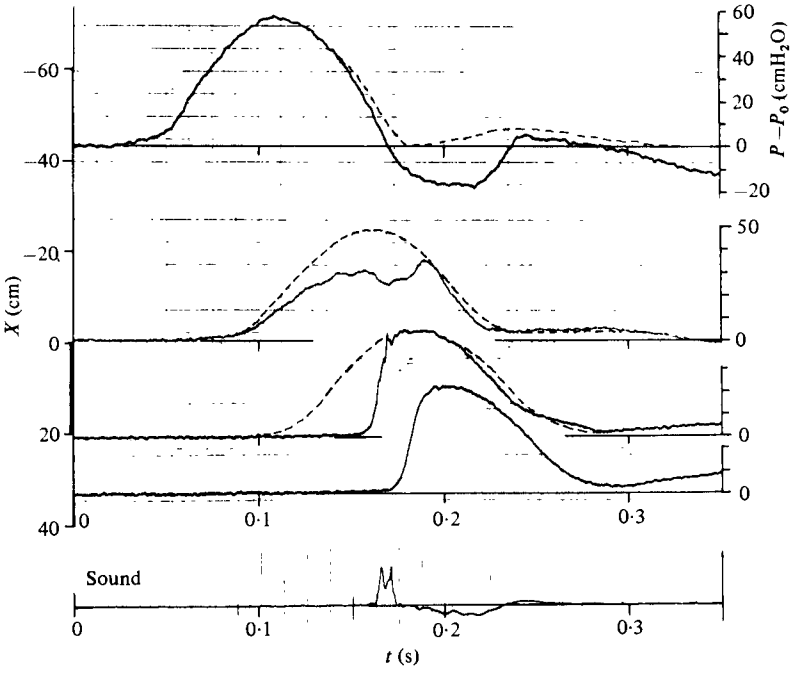

FIGURE 7. Measured pressure wave in the vicinity of the pressure box and sound monitored at the exit of the box; $L_b = 19$ cm, $P_0 = 40$, $P_{eb} = 40{\cdot}8$, $P_0 - P_{eb} = -0{\cdot}8$ cmH$_2$O. The top four figures are pressure and the bottom one is sound. Measuring site, from top to bottom, $X = -44$, $-1{\cdot}5$, $20{\cdot}5$, $35{\cdot}5$, $20{\cdot}5$ cm.

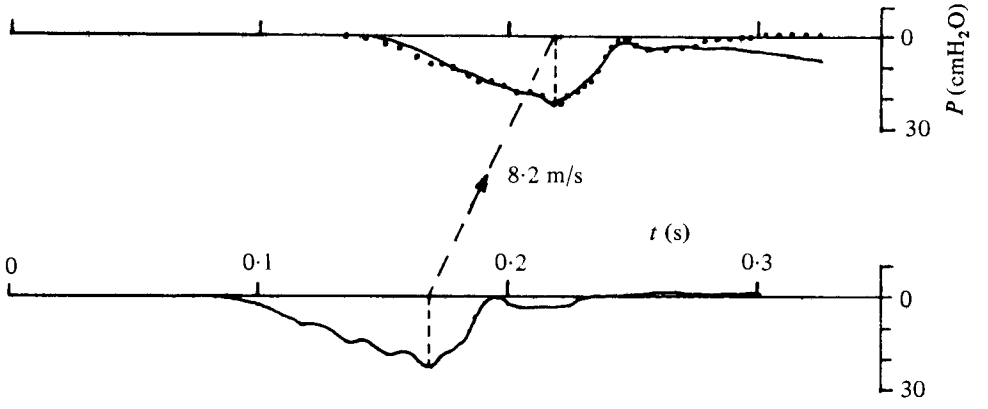

FIGURE 8. Graphically determined reflection wave produced by the partially collapsed tube segment in the box and its propagation velocity: top, $X = -44$ cm; bottom, $X = -1{\cdot}5$ cm.

the fluid-particle velocity. From these results, it can be seen that the incident pressure wave, generated by the pump, is partly reflected as a negative-pressure wave by the partially collapsed tube segment.

The pressure wave transmitted to the fully inflated tube segment distal to the pressure box consists of the steep ascending limb and the smooth remaining part. Synchronized with the steep ascending limb, strong sound is detected by the microphone. In this case, the sound can be heard by the ear as a thud sound. The relation between pressure wave and sound will be discussed in §3.3. It is interesting that the smooth portion of the transmission wave is almost identical with that of the

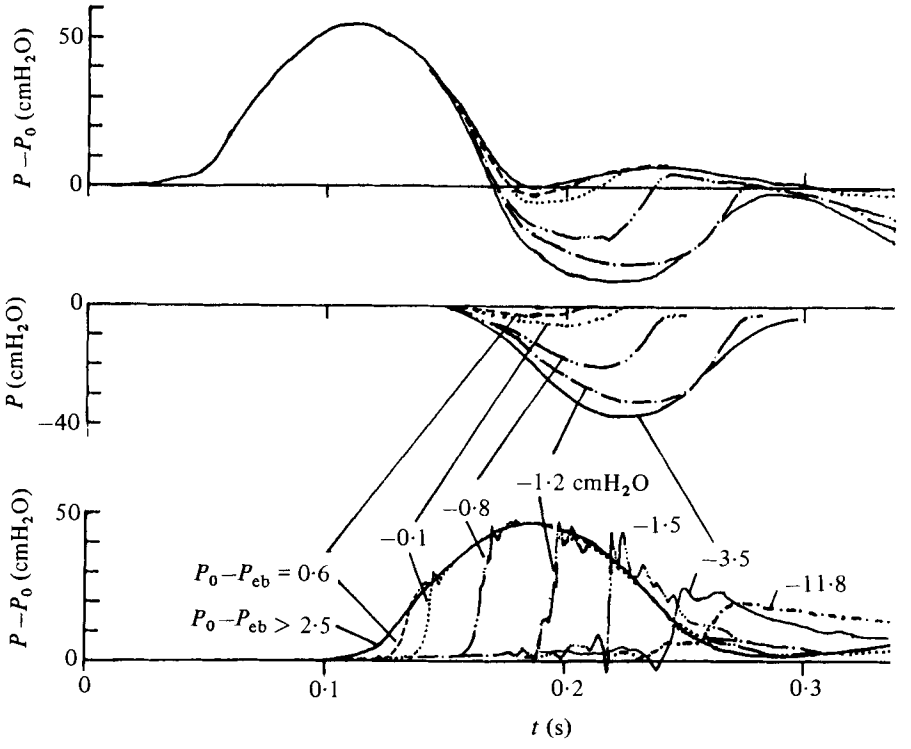

FIGURE 9. Effect of P_{eb}; L_b = 19 cm, P_0 = 40 cmH$_2$O: top, pressure wave measured at $X = -44$ cm; middle, graphically determined reflection wave at $X = -44$ cm; bottom, pressure wave measured at X = 20·5 cm.

fully inflated tube. Therefore, it can be said that the partially collapsed tube segment deforms the transmission wave so that some of the front portion of the incident pressure wave is cut off to make the steep ascending limb and the rest of it is untouched.

The effect of the degree of initial tube collapse on the transmission-wave deformation was examined. The measured pressure waves at the reference site ($X = -44$ cm) and the exit of the box (20·5 cm) and the graphically obtained reflection waves at the reference site are shown in figure 9 for various $P_0 - P_{eb}$. All the experimental conditions except P_{eb} are the same as those in figure 6. Regardless of the great external pressure difference in and out the pressure box, when $P_0 - P_{eb}$ is greater than 2·5 cmH$_2$O and hence the tube segment in the box is inflated, no significant pressure-wave deformation is detected. But, if $P_0 - P_{eb}$ descends below this value and the tube segment begins to collapse, the ascending limb of transmission wave becomes steep and at the same time the negative reflection wave in the proximal direction appears. With decrease of $P_0 - P_{eb}$, the reflection wave is augmented, and as a result the incident wave front portion seeming to be cut off by the steep ascending limb widens. However, if $P_0 - P_{eb}$ goes down below some value, in this case −1·2 cmH$_2$O, the deformed transmission wave is delayed as a whole from that of the fully inflated tube case and, at the same time, the form of the reflection wave ceases to be similar. With further drop of $P_0 - P_{eb}$, the transmission wave becomes weak and widely spread, and the amplitude of the negative reflection wave, not shown in the figure, decreases.

In addition to the abovementioned large-scale deformation, high-frequency pressure waves of the kind observed by Erlanger (1921) and Bramwell (1925) appear

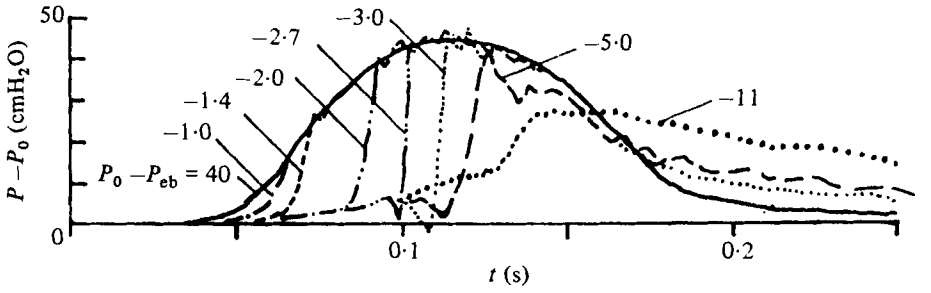

FIGURE 10. Measured pressure wave at 1·5 cm distal to 9 cm long pressure box for various P_{eb}; L_b = 9 cm, P_0 = 40 cmH$_2$O, X = 10·5 cm.

on the transmission wave along with the development of the steep ascending limb. When the steep ascending limb is low, they are weak and seen only just behind the ascending limb, but with the growth of the ascending limb they become strong and can be observed even over and in front of the ascending limb. These high-frequency pressure waves damp very rapidly in the fully inflated tube.

In order to see the effect of the collapsed-tube segment length L_b on the transmission-wave deformation, the same experiment was conducted using the shorter pressure box of 9 cm length. The pressure waves measured at the exit of the box (X = 10·5 cm) for various $P_0 - P_{eb}$ are shown in figure 10. All the experimental conditions except L_b are the same as those in figure 9. General characteristics of pressure-wave deformation are the same in both cases, but shortening of L_b makes the high-frequency pressure waves weak and lowers the $P_0 - P_{eb}$ value at which an identical transmission wave (with the same amplitude of ascending limb) is obtained at the exit of the box. In other words, the shorter the collapsed-tube segment, the higher becomes the P_{eb} which develops the steep ascending limb strong enough to generate an audible thud sound; the shorter the cuff, the higher the diastolic pressure estimated by the auscultatory technique. This agrees well with the fact reported by Kirkendall *et al.* (1967): 'if the cuff is too wide, the reading will be erroneously low'. And Steinfeld, Alexander & Cohen (1974) showed that there are significant errors if the cuff is too *short*.

3.3. *Relation between pressure wave, tube-wall movement and sound*

In §3.2 it has been shown that a transmission wave through the partially collapsed tube segment has a steep ascending limb and a strong sound is generated in a short period synchronizing with the ascending limb. In this subsection the mechanism by which the clear thud sound is generated by the steep ascending limb will be discussed.

Let us consider the sound generated by the fully inflated rubber tube outside the pressure box. As is well known, the amplitude S of a sound produced by an expanding or contracting elastic tube is proportional to the radial velocity V_w of the tube wall:

$$S \propto V_w = \frac{dr}{dt}, \tag{1}$$

where r is the radius of the tube. Using the relation between r and the cross-sectional area A

$$S \propto \frac{1}{A^{\frac{1}{2}}} \frac{dA}{dt}. \tag{2}$$

Assuming the static-tube law (figure 3) to be valid in the dynamic case, A is known to be almost linearly proportional to the transmural pressure $P - P_e$ for the fully

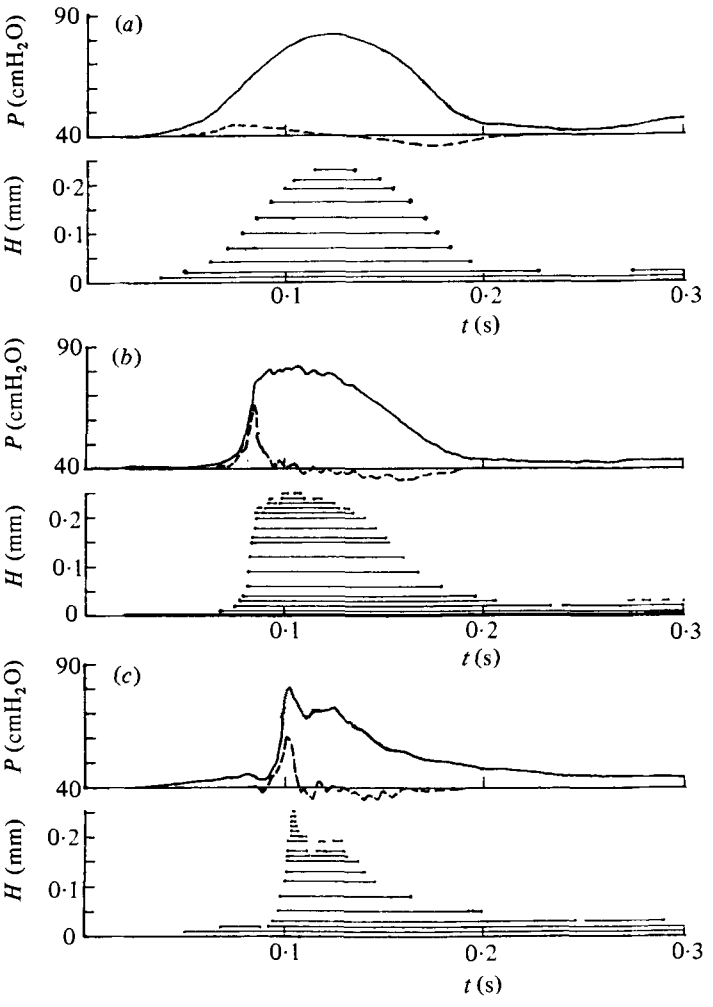

FIGURE 11. Movement of tube-wall top and sound due to transmission wave at 5 cm distal to the pressure box; $L_b = 9$ cm, $P_0 = 40$ cmH_2O, $X = 14$ cm: ——, pressure; – – –, sound; •——•, wall movement. (*a*) $P_{eb} = 0$, (*b*) $P_{eb} = 42$, (*c*) $P_{eb} = 45$ cmH_2O.

inflated tube. Since outside the box P_e is constant

$$\frac{dA}{dP} = K = \text{const.} \tag{3}$$

Introducing (3) into (2),

$$S \propto \frac{K}{A^{\frac{1}{2}}} \frac{dP}{dt}. \tag{4}$$

Assuming that the change in A due to the pressure wave is small,

$$S \propto \frac{K}{A_0^{\frac{1}{2}}} \frac{dP}{dt}, \tag{5}$$

where A_0 is the value at $P = P_0$. Equation (5) indicates that the amplitude of the sound is in proportion to time derivative of the pressure. Therefore if a pressure wave consists of a steep ascending limb and smooth remaining part a strong sound is generated only at the steep ascending limb.

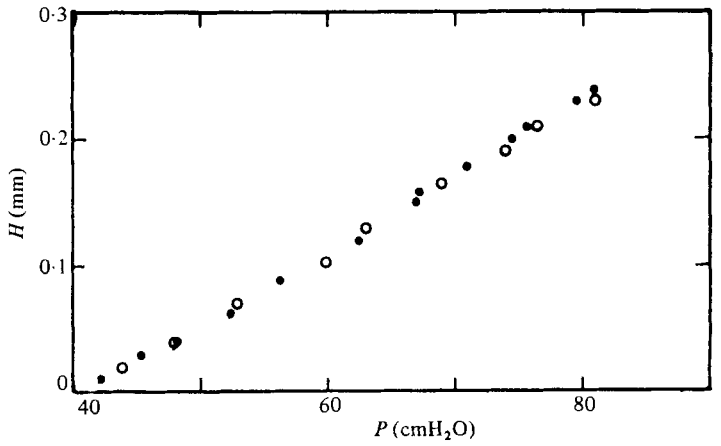

FIGURE 12. Relation between H and P on the ascending limb of the upper two figures in figure 11: ○, $P_{eb} = 0$; ●, $P_{eb} = 42$ cmH_2O.

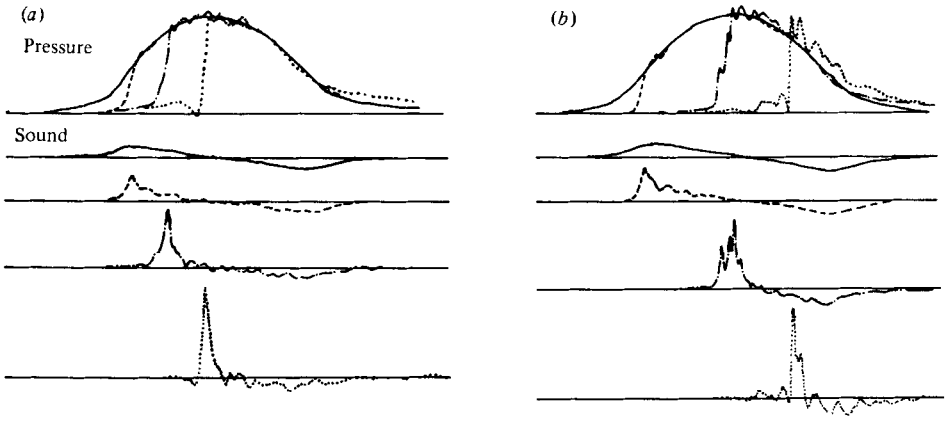

FIGURE 13. Comparison of pressure wave and sound measured simultaneously at the exit of the pressure box; $P_0 = 40$ cmH_2O, (*a*) $L_b = 9$ cm, $X = 14$ cm: ——, P_{eb} (cmH_2O) = 0; – – –, 41·4; —·—, 42·0; · · · ·, 43·0. (*b*) $L_b = 19$ cm, $X = 20{\cdot}5$ cm: ——, P_{eb} (cmH_2O) = 0; – – –, 39·5; —·—, 41·2; · · · ·, 41·5.

In order to check the reliability of this analysis, displacement of the tube upper wall due to a propagating pressure wave was measured. Some examples of transmission pressure wave P and the tube top-wall displacement H, simultaneously measured at 5 cm distal to the 9 cm long pressure box, are shown in figure 11. In the figure monitored sound waves are also shown by broken lines for reference. Since the tube is set on a solid horizontal surface, the displacement of the tube top wall H is equal to the tube-diameter variation. The maximum value of H is less than 0·25 mm, being very small compared with the initial tube diameter of 9 mm; therefore the assumption of small cross-sectional-area change is valid. The relation between H and P over the upstroke of the upper two figures is shown in figure 12. From the linear relation between H and P, (3) has been shown to be valid.

Some examples of simultaneously measured pressure and sound waves are shown in figure 13. The figure clearly shows that, as the steep ascending limb develops, the single positive sound becomes strong and sharp in its shape. When the collapsed tube segment is long, the high-frequency small pressure waves produce multipeaked sound.

Since the monitored sound waveform varied depending on the plastic-sleeve length attached to the microphone, the validity of (5) cannot be proved exactly by comparing the pressure and sound waves, but it is easily seen to be satisfied fairly well.

From these results, it has been shown that the clear thud Korotkoff sound at diastole is generated by sudden expansion of a blood vessel due to the steep ascending limb of the transmission pressure wave which is developed in the partially collapsed vessel segment under the cuff.

4. Calculation

In this section the mechanism by which the steep ascending limb of the transmission wave is produced will be shown by a one-dimensional numerical analysis simulating the experiment.

In order to simplify the problem, the following assumptions are made:

(i) the pressure-wave propagation phenomenon is one-dimensional;

(ii) the fluid filling the rubber tube is incompressible and inviscid;

(iii) the tube law obtained in static condition is valid even in a dynamic phenomenon.

The method of characteristics is a convenient measure to treat this kind of one-dimensional pressure-wave propagation problem (Kamm & Shapiro 1979) and the result greatly helps us to understand the behaviour of every part of the pressure wave. However, if pressure wave overtaking occurs as expected in the condition treated here and a discontinuous wavefront such as a shock appears, an unique solution cannot be determined any longer by the method, and it becomes necessary to adopt an appropriate condition in order to get the unique solution. So far, what fluid-dynamical phenomenon occurs at the shock developed in a collapsible tube by pressure-wave overtaking has not been understood well, and hence it cannot be determined what condition is most suitable. Some researchers (Beam 1968; Oates 1975) who treated shock formation by wave overtaking or a hydraulic jump in steady flow showed that there must be some energy loss at the shock. Their analysis, however, is developed on the assumption that the tube law, which is considered to be valid for pressure waves not so steep as shock (usually the statically obtained one as shown in figure 3), is also valid in the shock-wave region. As shown in the appendix, the amount of energy loss depends on the tube law for the shock (TLS); therefore, if the energy loss is taken into consideration, the selection of TLS is crucial. The TLS selected by the abovementioned researchers has been shown not to represent the real situation, as shown in the appendix. Since little is known about the fluid-dynamical phenomenon at the shock, what other TLS should be selected has not been determined, and furthermore it is not even known whether or not there is energy loss at the shock. However, judging from the experimental results conducted by Kececioglu *et al.* (1981), in which they measured pressure recovery across the stationary shock that is established in the collapsible tube when water flow jumps from a supercritical to subcritical condition, the energy loss at the shock formed by the wave overtaking is estimated to be very small. Therefore in our calculation the following assumptions are made: there is no energy loss at the shock wave and the shock propagates without changing its shape. The details of the shock treatment will be discussed in the appendix.

The assumptions adopted in the calculation, however, seem to become inadequate for the shocks with large tube cross-sectional-area change. As seen in the experimental

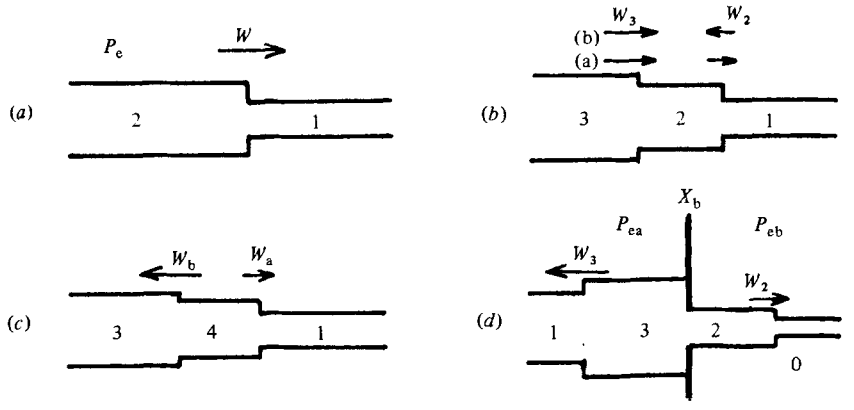

FIGURE 14. Schematic diagram explaining various occasions of step pressure wave propagation: (*a*) simple propagation; (*b*) before overtaking or meeting; (*c*) after overtaking or meeting; (*d*) at the P_e discontinuity location.

results, the shocks with large area change are accompanied by the high-frequency pressure waves, which are considered to be caused by axial tension and bending stiffness of the tube wall (McClurken *et al.* 1981) and seem to change the shape in the course of propagation. Therefore, in order to treat the shocks more realistically, more exact treatment including a realistic equation of motion of the tube wall may have to be introduced.

The equations determining the variables at the shock obtained from the above-mentioned assumptions, shown below as (8) and (10), become identical with the equations of the characteristics for a small-amplitude pressure wave. Therefore all the pressure waves, from small-amplitude wave to shock, can be treated by them without using the equations of characteristics, and hence the calculation is very simple and time saving.

The equations used in the calculation are reduced as follows. Let us consider, first, a step pressure wave propagating rightwards at velocity W through a uniform collapsible tube with constant uniform external pressure P_e, as shown in figure 14(*a*). Wave propagation velocity W and particle velocity U are defined to be positive towards the right. The variables in front of and behind the step are indicated by subscripts 1 and 2 respectively. The mass-conservation law and the integrated equation of motion are

$$\rho A_2(U_2 - W) = \rho A_1(U_1 - W), \tag{6}$$

$$\tfrac{1}{2}\rho(U_2 - W)^2 + P_2 = \tfrac{1}{2}\rho(U_1 - W)^2 + P_1, \tag{7}$$

where ρ is the density of the fluid in the tube. Eliminating W from (6) and (7),

$$U_2 - U_1 = \pm (P_2 - P_1)\left[\frac{2(A_2 - A_1)}{\rho(A_2 + A_1)(P_2 - P_1)}\right]^{\frac{1}{2}}, \tag{8}$$

where the + sign corresponds to a right-travelling wave and − to a left-travelling wave. Since the locations 1 and 2 belong to the non-shock region, the relation between A and P at those places should satisfy the statically obtained tube law

$$A = F(P - P_e). \tag{9}$$

From (8) and (9), if all the variables in front of the step and any one of them behind it are known, the state behind the step is known. Once those variables are known,

the wave-propagation velocity W is determined by (6), which is rewritten as

$$W = \frac{A_2 U_2 - A_1 U_1}{A_2 - A_1}. \tag{10}$$

Applying (8)–(10), overtaking and interaction of waves are treated as follows. When one wave overtakes or meets another one as shown in figure 14 (*b*), a pair of step waves propagating rightwards at velocity W_a and leftwards at W_b are produced, as shown in figure 14 (*c*). Expressing variables corresponding to each region by the subscripts shown in the figure and applying (8) to both waves,

$$\begin{aligned} U_4 &= U_3 - (P_4 - P_3)\left[\frac{2(A_4 - A_3)}{\rho(A_4 + A_3)(P_4 - P_3)}\right]^{\frac{1}{2}} \\ &= U_1 + (P_4 - P_1)\left[\frac{2(A_4 - A_1)}{\rho(A_4 + A_1)(P_4 - P_1)}\right]^{\frac{1}{2}}. \end{aligned} \tag{11}$$

Since the variables with subscripts 1 and 3 are all known, P_4, U_4 and A_4 are determined from (11) and (9) and W_a from (10).

Lastly, a step pressure wave passing through the tube, in which the external pressure changes discontinuously from P_{ea} to P_{eb} at X_b as shown in figure 14 (*d*), is considered. When a right-travelling step pressure wave 1 reaches the P_e discontinuous plane X_b, a reflection wave 3 and a transmission wave 2, which propagate leftwards and rightwards at velocity W_3 and W_2 respectively, are produced. At X_b, the flow is steady until the other wave reaches there; therefore steady mass-conservation law and Bernoulli's equation must be satisfied. The mass flow rates of waves 3 and 2 are determined by applying (8) multiplied by A_3 or A_2. Equating them

$$\begin{aligned} A_2\left\{U_0 + (P_2 - P_0)\left[\frac{2(A_2 - A_0)}{\rho(A_2 + A_0)(P_2 - P_0)}\right]^{\frac{1}{2}}\right\} \\ = A_3\left\{U_1 - (P_3 - P_1)\left[\frac{2(A_3 - A_1)}{\rho(A_3 + A_1)(P_3 - P_1)}\right]^{\frac{1}{2}}\right\}. \end{aligned} \tag{12}$$

From Bernoulli's equation

$$\begin{aligned} P_2 + \frac{\rho}{2}\left\{U_0 + (P_2 - P_0)\left[\frac{2(A_2 - A_0)}{\rho(A_2 + A_0)(P_2 - P_0)}\right]^{\frac{1}{2}}\right\}^2 \\ = P_3 + \frac{\rho}{2}\left\{U_1 - (P_3 - P_1)\left[\frac{2(A_3 - A_1)}{\rho(A_3 + A_1)(P_3 - P_1)}\right]^{\frac{1}{2}}\right\}^2. \end{aligned} \tag{13}$$

From the tube law

$$A_2 = F(P_2 - P_{eb}), \quad A_3 = F(P_3 - P_{ea}). \tag{14), (15}$$

As the variables with subscripts 1 and 0 are all known, P_2, A_2 and P_3, A_3 are determined by solving (12)–(15) simultaneously. U_2, U_3 and W_2, W_3 are also determined from (8) and (10) respectively.

Using these equations, propagation of a finite-amplitude pressure wave through an uniform tube, of which a portion is partially collapsed, was calculated by a computer and compared with the experimental results. In the following calculation the experimentally determined tube law (figure 3), approximated by many short straight-line segments, is used and the tube is assumed to be infinitely long. The initial condition, the pressure distribution along X at $t = 0$, is calculated from the experimentally obtained pressure wave at $X = -1{\cdot}5$ cm in a fully inflated tube case, which is approximated by 24 steps as shown in figure 15. The wall thickness of the

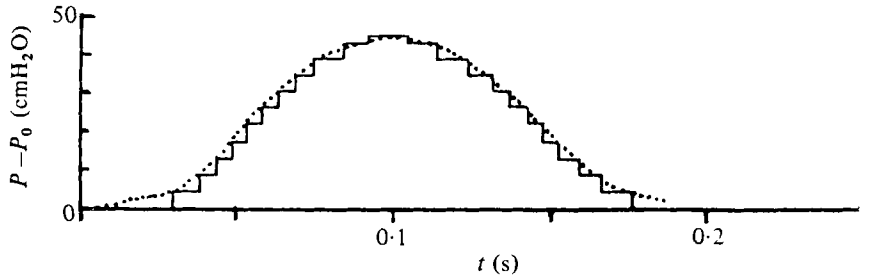

FIGURE 15. Approximation of incident pressure wave by 24 steps. ····, measured pressure wave at $X = -1{\cdot}5$ cm, $P_0 = 40$, $P_{eb} = 0$.

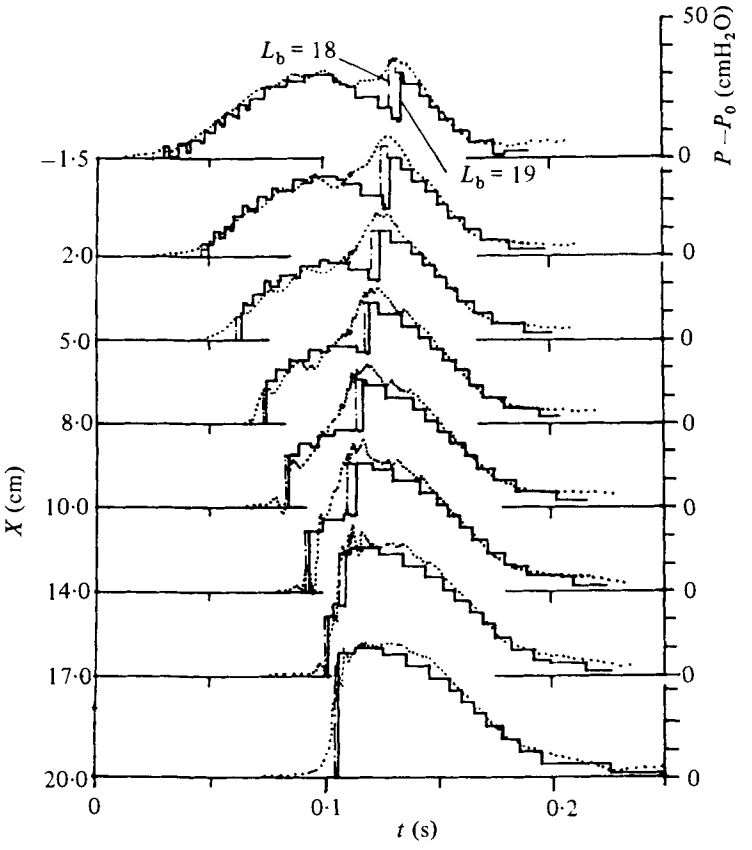

FIGURE 16. Comparison between calculated and measured pressure waves in and around the partially collapsed tube segment; $L_b = 19$ cm, $P_0 = 40$, $P_{eb} = 40{\cdot}8$, $P_0 - P_{eb} = -0{\cdot}8$ cmH$_2$O: ····, measured pressure; ——, calculated pressure, assuming $L_b = 19$; —·—, calculated pressure, assuming $L_b = 18$.

pressure box is neglected and the tube segment in the box is assumed to be collapsed uniformly. In some cases, however, in order to take the end effect of the collapsed tube segment into consideration, the effectively collapsed segment length is assumed shorter by 1 cm than the box length. Pressure waves smaller than 0·01 cmH$_2$O, produced by wave interaction or at P_e discontinuities, are neglected.

Calculated pressure waves at various locations within and outside the 19 cm long pressure box is shown in figure 16. In the figure, experimentally obtained pressure waves are also shown by dotted lines for comparison. The conditions of calculation

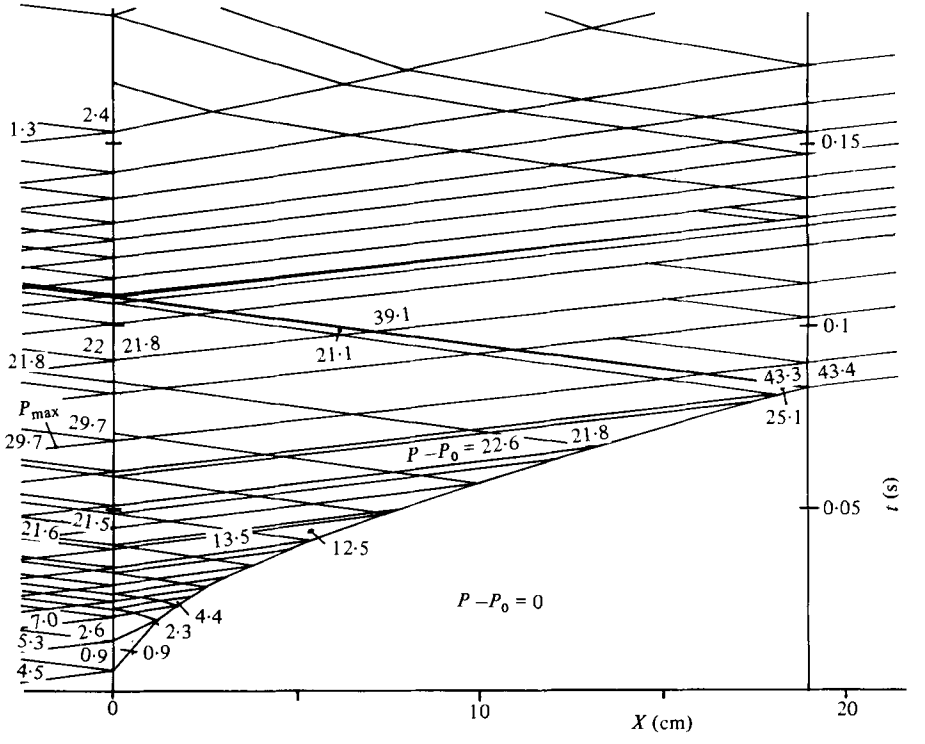

FIGURE 17. (X, t)-plane diagram showing propagation behaviour of each step pressure; $L_b = 19$ cm, $P_0 = 40$, $P_{eb} = 40{\cdot}8$, $P_0 - P_{eb} = -0{\cdot}8$ cmH_2O.

and experiment are the same as those in figure 7. Close similarity between the measured and the calculated pressure waves should be noted. The similarity is improved as shown by broken lines, if the effective collapsed tube segment length is assumed to be shorter by 1 cm than the pressure-box length. Deformation of the pressure wave in the collapsed tube segment is complicated. Let us see the behaviour of each step pressure wave indicated on a physical (X, t)-plane shown in figure 17. The numbers in the figure indicate the amplitude of pressure wave $P - P_0$. As the first incident step pressure wave reaches to the proximal end of the collapsed tube segment ($X = 0$), a strong negative reflection wave and a positive transmission wave are produced because of sudden change of the tube compliance. The pressure amplitude of the transmission wave is only 0·9 cmH_2O, but its cross-sectional-area change is relatively large, more than 13 %, and hence the step is called a shock wave. The second incident step pressure wave also produces at $X = 0$ a negative reflection and a positive transmission wave. This second transmission wave propagates faster (at 2·1 m/s) than the first one (0·9 m/s) because of the strong nonlinear characteristics of the tube law around zero transmural pressure, and soon overtakes the first one to make a stronger wave-front shock and, at the same time, a negative reflection wave. Each following step pressure wave repeats the same phenomenon. As seen in the figure, however, with increase of the incident pressure-wave amplitude, the amplitude of the transmission wave into the tube segment in the box increases and exceeds P_{eb}, and hence the initially collapsed tube segment becomes fully inflated. This reduces greatly the tube-complicance discontinuity at $X = 0$ despite the P_e difference, because the tube compliance is almost constant when $P - P_{eb}$ is greater than 5 cmH_2O (see figure 3).

This means that the reflection wave produced at $X = 0$ becomes very weak and the incident pressure wave propagates into the initially partially collapsed tube segment, without significant deformation, at the propagation velocity of the fully inflated tube. The propagation velocity of the wave-front shock increases with its growth, but it is still very low. Therefore it is continuously overtaken by the succeeding steps.

When the wave-front shock reaches the distal end of the collapsed tube segment a reflection and a transmission shock wave are produced. The former corresponds to the second hump of each pressure wave in figure 16 and the latter to the steep ascending limb of the transmission wave to the fully inflated distal tube. Thus it has been shown that the steep ascending limb which produces the thud Korotkoff sound is a shock wave built up within the partially collapsed tube segment.

As mentioned above, the high-amplitude portion of the incident wave propagates through the tube segment in the box without any deformation or delay; therefore the transmission wave recorded at the distal side of the pressure box has a shape consisting of the steep ascending limb (shock wave) and the intact incident wave portion following it.

As seen in figure 16, in the real situation the small high-frequency pressure waves appear in the course of the wave-front shock development, but not in the calculation. The difference is caused by the assumptions set for the calculation.

The effect of the collapsed tube segment length L_b is easily seen from figure 17; that is, if L_b is shorter than some critical value L_{bc} at which transmission wave corresponding to P_{max} overtakes the wave-front shock, the longer is L_b, then the greater is the amplitude of the wave-front shock, but, for L_b longer than L_{bc}, the wave-front shock amplitude decreases with increasing L_b, because of the expansion wave overtaking the wave-front shock.

In order to check the effect of the external pressure P_{eb}, a calculation has been done for various P_{eb}. When $P_0 - P_{eb}$ is greater than 4·0 cmH_2O, the compression-wave propagation velocity does not depend so strongly on $P - P_{eb}$ that overtaking occurs in the segment, therefore no significant wave deformation is observed. Below this $P_0 - P_{eb}$ value, however, the propagation velocity depends strongly on $P - P_{eb}$, and hence the wave-front shock formation occurs even in the short collapsed tube segment. Some examples of the calculated pressure wave with wave-front shock at the exit of the 19 cm pressure box are shown in figure 18. In the figure experimental results are also shown by dotted lines. The close resemblance between the two results should be noted. In the range of $P_0 - P_{eb}$ shown in the figure, the propagation velocity at the wave front decreases rapidly with decreasing $P_0 - P_{eb}$, therefore the amount of the successive pressure wave overtaking the wave-front shock increases with decreasing $P_0 - P_{eb}$, and, corresponding to this phenomenon, the shock strength at first increases and then decreases.

It is interesting that the one-dimensional calculation is valid even when $P_0 - P_{eb} = -2{\cdot}0$ cmH_2O, where the initial cross-sectional area of the collapsed segment is below one-half of that of the fully inflated segment, and hence the cross-sectional-area ratio at the wave-front shock becomes as large as 2·0. The (X, t)-plane diagram at $P_0 - P_{eb} = -2{\cdot}0$ is shown in figure 19. The wave-front shock propagation is very slow compared with that in figure 17, and the expanding pressure-wave portion of the incident wave overtakes the wave-front shock over the distal half of the collapsed segment. In the case of the expansion wave overtaking, the wave-front shock weakens and, at the same time, positive reflection waves are produced and the shock-propagation velocity slows down. Even in this case, the highest-amplitude portion of the incident wave propagates at about the same velocity as in the fully

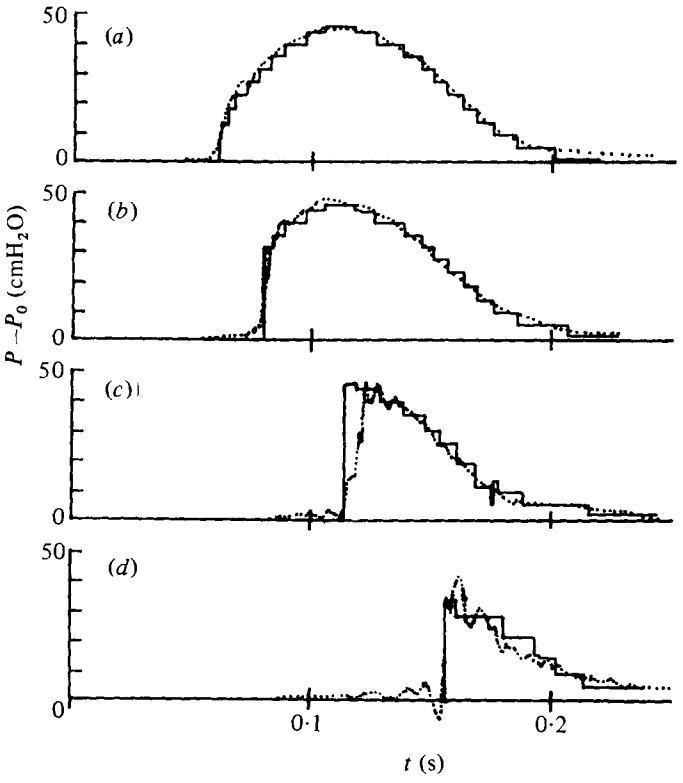

FIGURE 18. Comparison between calculated and measured pressure waves at the exit of the 19 cm pressure box; $P_0 = 40$ cmH_2O, $X = 20{\cdot}5$ cm: (*a*) $P_{eb} = 39{\cdot}5$; (*b*) 40·5; (*c*) 41·2; (*d*) 42·0 cmH_2O.

inflated tube, but its hind low-amplitude portion propagates more slowly because the tube segment again collapses partially, corresponding to the low-amplitude portion. This slow propagation causes the abovementioned delay of the transmission wave. As seen in the figure, the propagation velocity recovers after interaction with the reflected shock, therefore if the tube length is short (say 9 cm) and the shock reflection occurs early, no delay of the transmission wave is caused even in this $P_0 - P_{eb}$ condition, as seen in figure 10.

5. Conclusion

The following facts are evident from the abovementioned experimental and calculation results.

(i) The thud Korotkoff sound at diastole is generated by sudden expansion of the tube, corresponding to the very steep ascending limb of the transmission wave.

(ii) The steep ascending limb is a wave-front shock which is built up very rapidly in the partially collapsed tube segment under the compression cuff by the active overtaking phenomenon due to the strong nonlinear tube-law characteristics around zero transmural pressure.

(iii) Because of the nonlinear tube law, the incident wave behind the wave-front shock propagates through the initially collapsed tube segment without significant deformation; therefore the transmission waves to the distal inflated tube have a shape consisting of the shock and the intact incident wave portion following the shock.

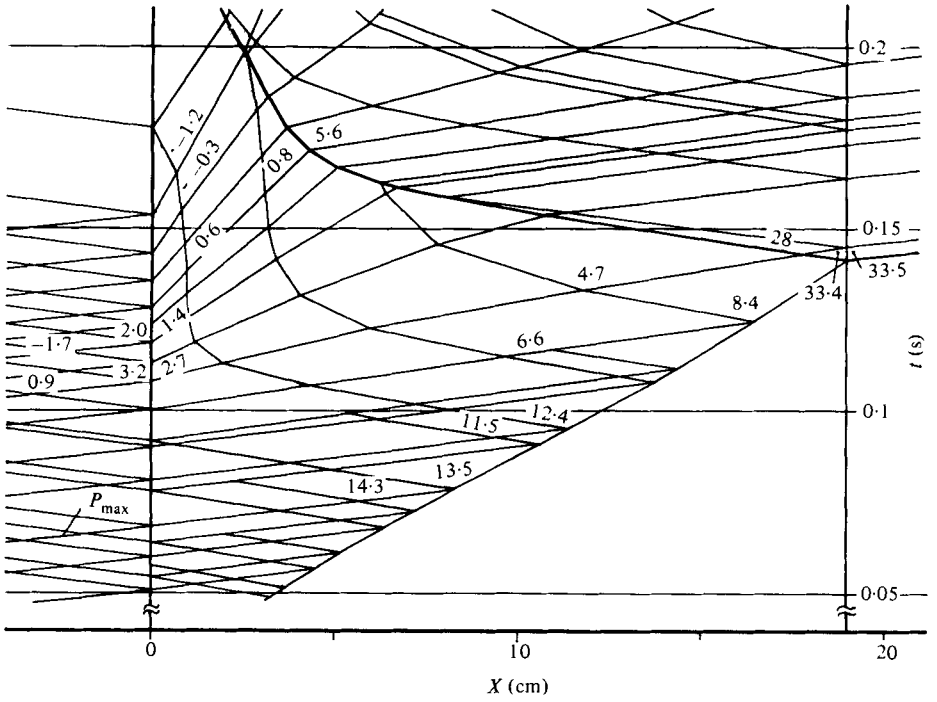

FIGURE 19. (X,t)-plane diagram for high collapse grade: $L_b = 19$ cm, $P_0 = 40$, $P_{eb} = 42{\cdot}0$, $P_0 - P_{eb} = -2{\cdot}0$ cmH_2O.

(iv) If the tube collapse grade is kept constant, the shock wave becomes stronger up to P_{max} with increasing collapsed tube segment length and becomes weaker with further increase of the segment length.

(v) The collapse grade shows a similar effect with the collapsed segment length, if the grade is below some limit.

We would like to thank the referees for their useful comments and suggestions.

Appendix

When the wavelength of the pressure wave is large enough compared to the tube diameter (non-shock wave) the flow in the tube is fairly well expressed by the following constitutive equations (Kamm & Shapiro 1979):

$$\frac{\partial A}{\partial t} + \frac{\partial (Au)}{\partial x} = 0, \tag{A 1}$$

$$\frac{\partial u}{\partial t} + u\frac{\partial u}{\partial x} = -\frac{1}{\rho}\frac{\partial P}{\partial x}, \tag{A 2}$$

$$A = F(P - P_e) \quad \text{or} \quad P = f(A). \tag{A 3}$$

Equation (A 3) is the tube law obtained in the static condition.

A non-shock compression wave generally steepens in the course of propagation and finally becomes a shock wave. Let us assume that the waveform of the shock does not change any further (assumption (i)). The number of conditions then becomes four,

(A 1)–(A 3) and assumption (i), and is greater by one than the number of dependent variables, P, u and A. Therefore to solve the problem it is necessary to take away one of the three equations (A 1)–(A 3) or to introduce one more dependent variable. Let us try to introduce the pressure loss ΔP as the new dependent variable. In the shock-wave region, the tube wall is greatly deformed in a short axial length; therefore it is more reasonable to consider that the tube law for the shock region is not identical with that for the non-shock region. Hence the general constitutive equations for the shock region are as follows:

$$\frac{\partial A}{\partial t}+\frac{\partial (Au)}{\partial x}=0, \tag{A 4}$$

$$\frac{\partial u}{\partial t}+u\frac{\partial u}{\partial x}=-\frac{1}{\rho}\frac{\partial P}{\partial x}-\frac{\Delta P}{\rho}, \tag{A 5}$$

tube law for shock region, (A 6)

$$\frac{\partial u}{\partial t}=-W\frac{\partial u}{\partial x} \tag{A 7a}$$

or

$$\frac{\partial A}{\partial t}=-W\frac{\partial A}{\partial x}, \tag{A 7b}$$

where W is the shock propagation velocity.

Introducing (A 7a, b) into (A 4) and (A 5) respectively,

$$-W\frac{\partial A}{\partial x}+\frac{\partial Au}{\partial x}=0, \tag{A 8}$$

$$-W\frac{\partial u}{\partial x}+u\frac{\partial u}{\partial x}=-\frac{1}{\rho}\frac{\partial P}{\partial x}-\frac{\Delta P}{\rho}. \tag{A 9}$$

Integrating (A 8) and (A 9) from plane 2 to plane 1 in figure 20(a),

$$A_1(u_1-W)-A_2(u_2-W)=0, \tag{A 10}$$

$$\int_2^1 \Delta P dx=(P_2-P_1)+\tfrac{1}{2}\rho\{(u_2-W)^2-(u_1-W)^2\}. \tag{A 11}$$

If the energy loss is zero, these equations become the same as (6) and (7). The equations (A 10) and (A 11) are also the mass- and momentum-conservation equations for the stationary shock as shown in figure 20(b). Let us try to relate the energy loss over the shock region, the left-hand term of (A 11), to the integrated pressure over the shock region. The integrated form of the momentum equation for the stationary shock is

$$A_2\{P_2+\rho(u_2-W)^2\}=A_1\{P_1+\rho(u_1-W)^2\}+\int_{A_1}^{A_2} P dA. \tag{A 12}$$

Putting $u_2-W=U_2, \quad u_1-W=U_1,$

(A 10) and (A 12) become

$$A_1 U_1=A_2 U_2=Q, \tag{A 13}$$

$$A_2(P_2+\rho U_2^2)=A_1(P_1+\rho U_1^2)+\int_{A_1}^{A_2} P dA, \tag{A 14}$$

where Q is the volume flow rate. As at planes 1 and 2 the tube law for the non-shock region should be satisfied

$$P_2=f(A_2);$$

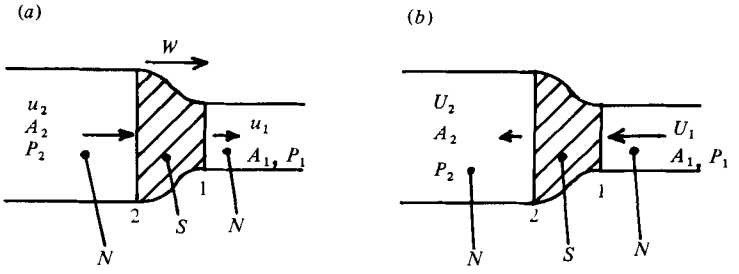

FIGURE 20. Diagrams of moving and stationary shock wave: (*a*) shock wave moving rightward at velocity W; (*b*) stationary shock observed from the coordinate system moving with shock. N, non-shock region; S, shock region. 1 and 2, boundaries between non-shock and shock region.

from this equation and (A 13) and (A 14)

$$A_2\left(f(A_2)+\rho\frac{Q^2}{A_2^2}\right) = A_1(P_1+\rho U_1^2)+\int_{A_1}^{A_2} P\,dA. \tag{A 15}$$

Therefore if the tube law in the shock region (TLS) is given then A_2 is determined from (A 15).

Now, using the abovementioned notation, the energy loss at the shock derived from (A 11) is

$$-\Delta E \equiv \int_2^1 \Delta P dx = (P_2-P_1)+\tfrac{1}{2}\rho(U_2^2-U_1^2). \tag{A 16}$$

Introducing (A 13) and (A 14) into (A 16),

$$-\Delta E = -\frac{\rho U_1^2}{2}\left(1-\frac{A_1}{A_2}\right)^2+\underbrace{\frac{1}{A_2}\left\{\int_{A_1}^{A_2} P\,dA-P_1(A_2-A_1)\right\}}_{\text{REC}}. \tag{A 17}$$

Equation (A 17) tells us that the amount of energy loss at the shock ΔE depends on the tube law in the shock region (TLS). The only experimental study that can be used to discuss the suitable TLS is that of Kececioglu *et al.* (1981). So let us consult the experimental results. To do so, some preparation is necessary.

From (A 17), the energy loss at the shock wave, across which the tube cross-sectional area changes from A_1 to A_2, depends on the second term on the right-hand side, named REC. When the tube law is expressed as shown in figure 21, the term REC is the area surrounded by the TLS, the horizontal $P = P_1$ line and the vertical $A = A_2$ line. Though the process is not shown here, the TLS for the loss-free condition ($\Delta E = 0$) is determined from (A 13), (A 14) and (A 16), or $P'(A)+\frac{1}{3}AP''(A) = 0$ (Kamm & Shapiro 1979) as

$$P = -\frac{A_1^2A_2^2(P_2-P_1)}{A_2^2-A_1^2}\frac{1}{A^2}+\frac{P_2A_2^2-P_1A_1^2}{A_2^2-A_1^2}, \tag{A 18}$$

and shown in figure 21 by a broken line. In this case REC is largest. When the Borda–Carnot condition (that is $P = P_1$ over the shock region) is selected as TLS, the term REC becomes zero, and hence ΔE is maximum. When the statically obtained tube law is selected as TLS, as done by Oates (1975), the amount of REC is the hatched area in figure 21 and the energy loss is relatively large. Now, let us relate the REC term and the experimental results of Kececioglu *et al.* (figure 16 in their paper). The term C_p used by them is

$$C_p = \frac{P_2-P_1}{\frac{1}{2}\rho U_1^2}. \tag{A 19}$$

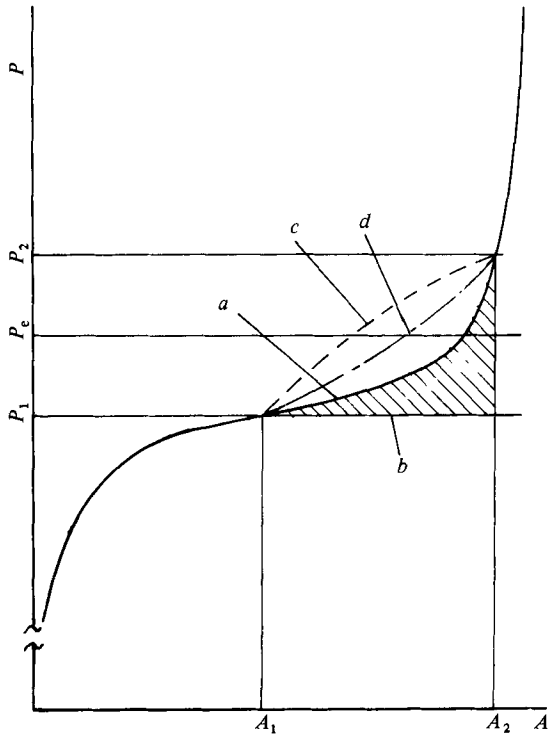

FIGURE 21. Tube laws in the shock region representing various hypotheses. (*a*) statically obtained tube law; (*b*) Borda–Carnot condition; (*c*) tube law for loss-free shock; (*d*) tube law for steady-flow hydraulic jump.

Introducing (A 16) and (A 13) into (A 19),

$$C_p = \frac{\Delta E}{\frac{1}{2}\rho U_1^2} + 1 - \left(\frac{A_1}{A_2}\right)^2; \tag{A 20}$$

and introducing (A 17) into (A 20)

$$C_p = 2\frac{A_1}{A_2}\left(1 - \frac{A_1}{A_2}\right) + \frac{\text{REC}}{\frac{1}{2}\rho U_1^2 A_2}. \tag{A 21}$$

When the Borda–Carnot condition is selected as TLS, C_p is equal to the first term on the right-hand side of (A 21), and expressed by $C_{p\,\text{B-C}}$ in their figure. When the statically obtained tube law is selected as TLS (Oates' case) there is some pressure recovery, and C_p, expressed by C_{p0} in their figure, is a little bit larger than $C_{p\,\text{B-C}}$. But, according to the figure, almost all the experimental results, except the long-type shock, are greater than C_{p0}. Therefore the amount of REC is much greater than that in Oates' case. This means that the TLS that suits the experimental condition of Kececioglu *et al.* is between those for the loss-free case and for Oates' case, something like the one shown by a chain line in figure 21. Since Kececioglu *et al.* measured pressure recovery across the stationary shock that is established in the collapsible tube when the water flow jumps from a supercritical to a subcritical condition, there must be some flow separation at the stationary shock, which causes great energy loss. In the case of a moving shock, treated in this report, the flow observed from the coordinate system fixed to the shock becomes similar to that of

Kececioglu *et al.* In the moving-shock case, however, the real flow direction is opposite to the stationary-shock case, and hence the velocity profiles in their boundary layers are quite different. That is, in the moving-shock case, the maximum velocity appears at the tube wall, which moves at the propagation velocity of the shock. In the flow of this kind, no flow separation at the shock is expected. Therefore the energy loss is considered to be smaller in the moving-shock case than in the stationary case. This means that TLS suitable for the moving shock may approach closer to the one for a loss-free condition in figure 21. Based on these considerations, the loss-free assumption for the shock wave is considered to be a good approximation.

REFERENCES

ALEXANDER, H., COHEN, M. L. & STEINFELD, L. 1977 *Med. Biol. Engng Comput.* **15**, 2.

ANLIKER, M. & RAMAN, K. R. 1965 *Int. J. Solids Structures* **2**, 467.

BEAM, R. M. 1968 *NASA TN* D-4803.

BRAMWELL, J. C. 1925 *Heart* **12**, 23.

BROWER, R. W. & SCHOLTEN, C. 1975 *Med. Biol. Engng* **13**, 839.

BURNS, P. L. 1959 *Am. J. Med.* **27**, 360.

CHUNGCHAREON, D. 1964 *Am. J. Physiol.* **207**, 190.

ERLANGER, J. 1921 *Am. J. Physiol.* **55**, 84.

FRUEHAN, C. T. 1962 *New Physician* **11**, 433.

KAMM, R. D. & SHAPIRO, A. H. 1979 *J. Fluid Mech.* **95**, 1.

KECECIOGLU, I., MCCLURKEN, M. E., KAMM, R. D. & SHAPIRO, A. H. 1981 *J. Fluid Mech.* **109**, 367.

KIRKENDALL, W. M., BURTON, A. C., EPSTEIN, F. H. & PREIS, E. D. 1967 *Circulation* **36**, 980.

KOROTKOFF, N. S. 1905 *Rep. Imp. Med. Acad., St Petersburg* **2**, 365.

LIGHTHILL, M. J. 1972 *J. Fluid Mech.* **52**, 475.

MCCLURKEN, M. E., KECECIOGLU, I., KAMM, R. D. & SHAPIRO, A. H. 1981 *J. Fluid Mech.* **109**, 391.

MCCUTCHEON, E. P. & RUSHMER, R. F. 1967 *Circulat. Res.* **20**, 149.

OATES, G. C. 1975 *Med. Biol. Engng* **13**, 773.

PICKERING, G. W. 1955 *High Blood Pressure.* Grune & Satton.

STEINFELD, L., ALEXANDER, H. & COHEN, M. L. 1974 *Am. J. Cardiol.* **33**, 107.

UR, A. & GORDON, M. 1970 *Am. J. Physiol.* **218**, 524.

WALLACE, J. D., LEWIS, D. H. & KHALIL, S. A. 1961 *J. Acoust. Soc. Am.* **33**, 1178.